Available online at www.sciencedirect.com
ScienceDirect
Aerospace Science and Technology 11 (2007) 507–517
Aerospace Science and Technology
www.elsevier.com/locate/aescte

Steady and unsteady numerical investigation of transitional shock-boundary-layer-interactions on a fan blade ☆

Stationäre und instationäre numerische Untersuchung von transitionalen Stoß-Grenzschicht-Interaktionen an einer Fanschaufel

B. Becker [a,*], M. Reyer [b], M. Swoboda [a]

[a] *Rolls-Royce Deutschland Ltd & Co KG, Eschenweg 11, 15827 Blankenfelde-Mahlow, Germany*
[b] *TU-Berlin, Institut für Luft- und Raumfahrtechnik, Marchstraße 12-14, 10587 Berlin, Germany*

Received 28 November 2006; received in revised form 29 March 2007; accepted 2 May 2007

Available online 5 May 2007

Abstract

The present numerical study was performed to investigate the impact of both the Reynolds number variation and the used turbulence model to capture the boundary layer development on the characteristic of a BR710 fan blade. A one-equation model of Spalart Allmaras with an optional semi-empirical transition model of Abu-Ghanam Shaw has been applied. The transition model allows the boundary layer development from a laminar to a turbulent behaviour to be taken into account. This is of particular importance at low Reynolds numbers and thus high operating altitudes of airplanes when the transition location moves further downstream to the trailing edge. Therefore the interaction between the shock waves of the transonic fan blade row and the boundary layer leads to a significant change of the characteristic. The steady numerical studies of the 3-D blade passage have been carried out with the commercial 3-D Navier–Stokes solver NUMECA. Additionally an unsteady calculation has been applied to explain the penalty in efficiency on high operating altitudes.

Zusammenfassung

Die vorliegende numerische Arbeit wurde durchgeführt, um den Einfluss einer Reynoldszahlveränderung und die Verwendung unterschiedlicher Turbulenzmodelle zur Modellierung der Grenzschichtentwicklung auf die Kennlinie des BR710 Fans zu untersuchen. Dabei kam ein Eingleichungsmodell von Spalart Allmaras mit einer optionalen Erweiterung eines halbempirischen Transitionsmodells von Abu-Ghanam Shaw zum Einsatz. Die Verwendung des Transitionsmodells ermöglicht die Berücksichtigung der Grenzschichtentwicklung vom laminaren zum turbulenten Zustand. Dies ist für geringe Reynoldszahlen, wie sie in großen Flughöhen von Flugzeugen auftreten, von besonderer Bedeutung, da sich die Transition der Grenzschicht weiter stromabwärts auf der Fanschaufel vollzieht. Als Folge daraus führt die Interaktion zwischen den Stoßwellen und der Grenzschicht der transsonischen Fanstufe zu einer signifikanten Veränderung der Kennlinie. Die stationären numerischen Untersuchungen der 3-D Schaufelpassage wurden mit Hilfe des kommerziellen 3-D Navier–Stokes-Gleichungslösers NUMECA durchgeführt. Zusätzlich wurde eine instationäre Lösung berechnet, um die beobachteten Wirkungsgradeinbußen bei großen Flughöhen zu erklären.

Keywords: Shock-boundary-layer-interaction; Fan; Transition; Reynolds number effect

Schlüsselwörter: Stoß-Grenzschicht-Interaktion; Fan; Transition; Reynoldszahl Effekt

☆ This article was presented at the German Aerospace Congress 2006.

* Corresponding author.
E-mail address: bernd.becker@rolls-royce.com (B. Becker).

1270-9638/$ – see front matter
doi:10.1016/j.ast.2007.05.002

Nomenclature

α	angle of attach	°	
c	chord length	m	
$C_f = \frac{\tau_w}{\frac{\rho}{2}U^2}$	skin friction coefficient		
$\text{sign}(\tau_{\text{wAx}})$	signum of wall shear stress in axial direction		
d	wall distance	m	
D/Dt	total derivative		
f	frequency	1/s	
g_t	grid spacing factor		
Γ	intermittency (0 = laminar, 1 = turbulent)		
$\eta_{\text{is}} = \frac{(\frac{\bar{P}_{\text{totOut}}}{\bar{P}_{\text{totInl}}})^{\frac{\kappa-1}{\kappa}}-1}{\frac{\bar{T}_{\text{totOut}}}{\bar{T}_{\text{totInl}}}-1}$	isentropic efficiency based on mass flow weighted total quantities		
M	Mach number		
$\dot{m}_{\text{red}} = \dot{m} \cdot \frac{\sqrt{\bar{T}_{\text{totInl}}}}{\bar{P}_{\text{totInl}}}$	flow function (total corrected mass flow)	$\frac{\text{kg}}{\text{s}}\frac{\sqrt{\text{K}}}{\text{kPa}}$	
ν	kinematic viscosity	m^2/s	
$\tilde{\nu}$	turbulent working variable	m^2/s	
$p^* = P_{\text{stat}}/P_{\text{totInl}}$	critical pressure ($M = 1$)		
$\Pi = \frac{\bar{P}_{\text{totOut}}}{\bar{P}_{\text{totInl}}}$	mass flow weighted pressure ratio		
Re	Reynolds number based on fan chord length		
ρ	density	kg/m^3	
s	surface coordinate	m	
s_0	surface length	m	
$\tilde{S}$	production term		
$S_r = \frac{c \cdot f}{U}$	Strouhal number		
t	time	s	
τ_{w}	viscous stress	N/m^2	
U	velocity	m/s	
$u_\tau = \sqrt{\frac{\tau_w}{\rho}}$	wall friction velocity	m/s	
$y^+ = \frac{u_\tau \cdot d}{\nu}$	non-dimension wall distance		

1. Introduction

The aim to increase the efficiency of propulsion turbojet engines motivated the designers of fan blades to reduce the pressure losses caused by the viscous effects along the blade surface and the shock losses. Recent airfoil designs are based on so-called transonic laminar profiles leading to a drag reduction of up to 15%. The boundary layer is kept in a laminar shape up to 50% of the cord length by active flow control or by the design of the blade to reach this benefit. This effect is also taken into account within the design process of a fan blade to increase the efficiency of the stage.

In order to take advantage of the effect it is necessary that the design tool provides for the laminar turbulent behaviour of the boundary layer. The transition from a laminar to a turbulent boundary layer has a serious impact on the overall drag and performance of the blade. The influence is increased when the Reynolds number is low.

This is the case for high operating altitudes. For example corporate jets operate at altitudes up to 51 kft to get a direct connection to their flight destination. Under these conditions the low density causes high kinetic viscosity and thus the Reynolds number decreases significantly. As a result the transition occurs further downstream on the blade, which leads to an extended length of the laminar boundary layer.

Compared to an airfoil the detached shock wave of a blade row enters the blade passage and interacts with the boundary layer of the adjacent blade. Depending on the Reynolds number and the shock angle the boundary layer can still be laminar when the shock impinges the boundary layer. In this case the interaction is stronger than in the turbulent case. The position of the boundary layer transition becomes unstable because of the interaction. This movement of the transition region has to be taken into account within the design process to prevent flutter problems.

2. Shock-boundary-layer-interaction

There are general differences between laminar and turbulent shock-boundary-layer interactions. Usually a laminar shock-boundary-layer interaction region is much more sensitive to a large pressure gradient than a turbulent one. Thus the flow can in this case not withstand the pressure increase and separates earlier. This causes performance and stability penalties. Furthermore it is well known that the unsteady shock oscillations are much more pronounced in the case of a laminar interaction. Knowledge of this makes it possible to perform a redesign of a fan blade, which is much less sensitive to laminar-turbulent transition effects. To represent the conditions of free flight in a wind tunnel test as realistically as possible, the transition from laminar to turbulent flow is, in most cases, fixed in the proximity of a profile leading edge by means of a transition strip. For traditional transonic airfoils, this assumption was correct because of its geometry and the resulting pressure distribution (front loading which results in strong positive pressure gradient).

In the work of Swoboda and Nitsche [10] a direct comparison of the flow around a transonic airfoil in fully turbulent (fixed transition) and transitional case is given. They use conventional field measuring techniques and advanced unsteady surface measuring techniques to clarify the differences, which occur during turbulent and transitional shock boundary-layer interactions.

Even when using conventional measuring techniques, large differences between laminar and transition-fixed flow can be observed. In order to illustrate this, the global flow field was measured by means of Laser-2-Focus anemometry in the middle section of an airfoil in a wind tunnel. A CAST7 airfoil was investigated here. The Reynolds number, which is based on profile chord of 0.1 m was 1.4 Million. Here, the same shock position that occurs in the two different flow fields was in the focus of interest. As a first and most important result, the free stream Mach numbers differ in the respective cases. As an example,

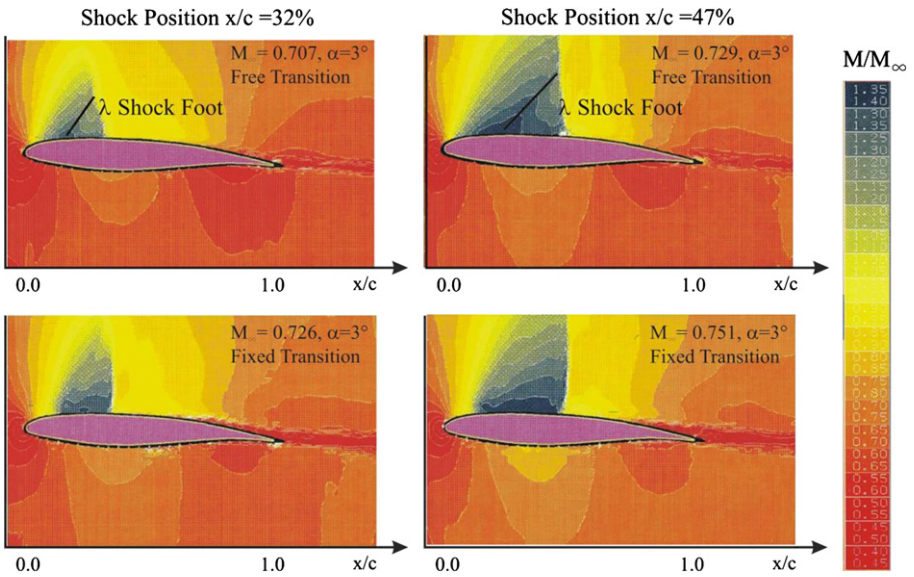

Fig. 1. Measured (L2F) Mach number distribution for a CAST 7 airfoil for laminar and fully turbulent boundary layers at two different shock positions.

the results of this Mach number measurements are presented in Fig. 1 (left) at a shock position of 32% of profile chord. Fig. 1 (right) shows the same result for a shock located further downstream at position of 47% chord. The differences between free and fixed transition are to be clearly seen. In the case of free transition, the flow accelerates regularly on the suction side into the supersonic region, but slows down as early as in the middle of this region above a front foot of a λ-shock, which is caused by the beginning of the separation bubble. Here, the beginning of the separation bubble has the same effect as a viscous ramp in the supersonic region. For this reason, the supersonic region is limited by means of a shock that is slightly curved in the upstream direction.

Concerning fixed transition, the flow is accelerated later on the suction side, and the supersonic region is limited by a more or less vertical (and therefore stronger) shock. Because of greater fluctuations, the supersonic region is also more fully developed above the airfoil in this case. Further downstream of the shock, a slight expansion behind the shock takes place in both cases. This expansion is much more distinct in the case of free transition.

All those effects described above are also valid for turbo machinery flows. Especially in fan blades the free stream turbulence is very low which avoids an early transition and might lead to a laminar boundary layer in the shock region. To promote early transition Ginder and Calvert [3] chose a suction side pressure distribution with flow deceleration to ensure that the boundary layer is turbulent when the shock attaches the fan blade. In this case they can assume a turbulent shock-boundary layer interaction. This is not the case in conventional designs where the location of the boundary layer transition is more influenced by the Reynolds number. In small fan blades the Reynolds number is lower and the shape and thickness of the leading edge becomes of particular importance for the transition location because of leading edge separation bubbles (Walraevens and Cumpsty [11]). Additionally there is no earlier transition expected as it is normally assumed in the scaled experiments for airfoils. The fan blades are tested in full scale and thus there is no need for a Reynolds number correction, which would move the transition point further upstream. Due to those effects the transition point of the boundary layer can vary and the interaction with the shock can change. But the transition location can also change because of the operating conditions. The operating range of a turbo machine can vary significantly from take off at atmospheric ambient conditions up to very high altitudes. Consequently, the variation of Reynolds numbers is very high within the operating range of a turbo machine and thus the effects described above are very important and have to be taken into account during the design of turbo machinery components.

3. Computational method

Within the frame of the presented computations a commercial CFD systems has been employed. FINE™/Turbo, developed by NUMECA Int. S.A, is a specialised CFD package for all types of turbomachinery applications. The package includes automatic structured grid generation, the flow solver and a post processing software. All program modules are embedded into a turbomachinery specific environment.

The numerical scheme solves the 3D Reynolds-averaged Navier–Stokes equations (RANS) on general structured non-orthogonal multi-block grids. The flexibility of the structured grids is greatly enhanced by use of so-called “Full Non Matching Connections”, a technique, which allows to arbitrarily connecting grids block of different grid topologies or point numbers to each other without numerical interpolation losses.

The numerical algorithm incorporated into FINE™/Turbo is an explicit four stage Runge–Kutta scheme (Jameson and Baker [5]). A variety of convergence acceleration techniques are employed, such as implicit residual smoothing, dual time stepping and a full multigrid algorithm. Space integration is performed using a second order cell-centred finite volume discretisation with second and fourth order artificial dissipation. Coarse grid

calculations can be carried out in an automatic way on every coarser grid level. A dual time stepping approach was used for the unsteady calculations.

A number of turbulence models are available within FINE™/Turbo. In the scope of the present work the one-equation low Reynolds number model of Spalart and Allmaras [9] has been chosen, in connection with a transition model. The location of the transition onset and the length of the transition region are based on a semi-empirical approach proposed by Abu-Ghanam and Shaw [1]. The implementation and the influence of the intermittency distribution was investigated by Hildebrandt et al. [4] on a 1,5 stage low speed compressor.

4. Transition model

For the simulations in the present work the one-equation turbulence model of Spalart and Allmaras [1] was used in combination with the transition model of Abu-Ghanam Shaw.

The one-equation turbulence model of Spalart–Allmaras models can be written as:

$$\frac{D\tilde{\nu}}{Dt} = c_{b1}[1 - f_{t2}]\tilde{S}\tilde{\nu} + \frac{1}{\sigma}\big[\nabla.\big((\nu + \tilde{\nu})\nabla\tilde{\nu}\big) + c_{b2}(\nabla\tilde{\nu})^2\big] - \left[c_{w1}f_w - \frac{c_{b1}}{\kappa^2}f_{t2}\right]\left[\frac{\tilde{\nu}}{d}\right]^2 + f_{t1}\Delta U^2 \tag{1}$$

where ν is the molecular kinematic viscosity and $\tilde{\nu}$ denotes the turbulent working variable (Spalart and Allmaras, [9]). The f_{t2} term has been introduced by Spalart and Allmaras in order to alter the production term so that a zero value of $\tilde{\nu}$ becomes a stable solution in the laminar region. This term can be written as:

$$f_{t2} = c_{t3}\exp(-c_{t4}\chi^2) \tag{2}$$

where $\chi = \tilde{\nu}/\nu$.

The last term on the right-hand side of Eq. (1) is the "trip" term, which promotes turbulence. It depends on ΔU, which is the norm of the difference between the velocity at the trip point and that at the field point considered, and on the f_{t1} function. The trip function can be written as:

$$f_{t1} = c_{t1}g_t\exp\left(-c_{t2}\frac{\omega_t^2}{\Delta U^2}\big[d^2 + g_t d_t^2\big]\right) \tag{3}$$

ω_t denotes the vorticity at the closest transition point, whereas d_t is the distance to this point. d is the distance to the solid wall. The g_t factor allows the shape of the ellipse to depend on the grid spacing along the wall at the trip:Δx_t. It is defined as:

$$g_t = \min\left(0.1, \frac{\Delta U}{\omega_t \Delta x_t}\right) \tag{4}$$

The model constants in this formulation are $c_{t1} = 10, c_{t2} = 2, c_{t3} = 1.2$, and $c_{t4} = 0.5$.

In order to apply this model in unsteady mode, re-laminarisation has to be allowed. One option is to introduce a so-called intermittency, Γ. It is defined as the fraction of time during which the flow over any point on a surface is turbulent. It should be zero in the laminar boundary layer and unity in a fully developed turbulent boundary layer. The intermittency is used to multiply the production term. For the Spalart–Allmaras turbulence model this leads to:

$$\tilde{S} = \Gamma\tilde{S} \tag{5}$$

Free-stream wakes (with only a weak production term) will not be affected by the intermittency. A laminar boundary layer will be preserved upstream of the transition location and turbulence could freely develop thereafter. As a default the intermittency is zero before transition and one after the transition onset (binary behaviour). Transition was therefore triggered, unnaturally, in an on-off manner. In order to gain more insight about the effect of intermittency Hildebrandt et al. [4] have performed calculations with an intermittency distribution according to Dhawan and Narasimha [2]. There are only small deviations compared to the non-intermittent results without an intermittency distribution. The transition onset is moved only slightly downstream in the case of a calculation with an intermittency distribution. The capabilities of the transition model were tested in a 4-stage compressor and compared with experimental results from Johann et al. [6]. Because of the good agreement of the predicted transition locations of the model with the measured transition locations on the (hot wire equipped) stators the transition model was used instead of the higher order models like the one of Menter et al. [8], which would lead to more detailed results.

5. Investigated fan blade

Most calculations were carried out on an early preliminary design of a BR710 fan blade. The conventional blade profiles were designed in house and are not comparable to precompression designs from Ginder and Calvert [3]. Therefore the results cannot be used to draw general conclusions for fan blades other than the small BR710 one. The BR710 engine, which powers a number of corporate jets, is equipped with a fan of 48 inch diameter. The jets equipped with this engine are designed to fly at very high altitude of up to 51.000 ft (15545 m). The atmospheric conditions at this altitude result in very low Reynolds numbers. To explore the differences between ambient sea level conditions and the flight at high altitude the fan blade was calculated at both conditions. The reduced rotational speed was kept constant in order to ensure comparable inlet conditions in terms of the Mach number. Below, the Reynolds numbers are depicted:

BR710 Fan	Sea Level:	$Re_{\text{sea}} = 2.3 \times 10^6$
BR710 Fan	51 kft Altitude:	$Re_{\text{alt}} = 5.06 \times 10^5$

6. Numerical grid

The mesh is a structured multi-block topology consisting of a total of 9 mesh blocks leading to an overall grid size of approximately 1.6 million grid points.

Fig. 2 shows the overall computational domain and the respective calculated passage. Further details of the grid are shown in Fig. 3 at the mid span position. The tip clearance gap

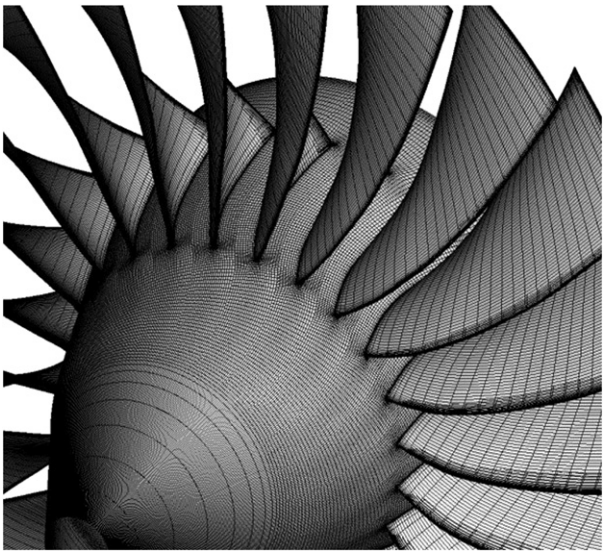

Fig. 2. BR710 fan blade coarse grid (skip = 2), repetition.

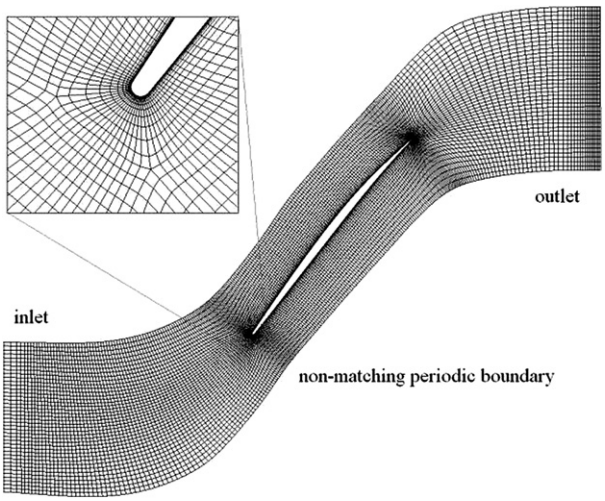

Fig. 3. Grid at mid span in blade to blade view and boundary conditions for the computational domain.

is resolved quite finely with 17 radial grid points to resolve the tip clearance vortex flow.

The Spalart–Allmaras turbulence model is used in a low-Reynolds formulation without wall functions requiring a fine mesh resolution to ensure at least a few cells inside the viscous sublayer. Consequently, the non-dimensional wall distance should be in the range of values within the viscous sublayer verified by Fig. 4 for the calculation with fully turbulent treatment of the boundary layer (Spalart–Allmaras) under sea level (high *Re*) conditions (rotor at midspan).

Since the y^+-values are directly correlated with the wall shear stress, a transition location can be observed on these values, because higher levels of wall shear stress result in higher y^+-values. On the suction side (SS) the step in y^+ occurs at $s/s_0 = 0.55$ whereas the transition on the pressure side (PS) is located at $\sim s/s_0 = 0.3$.

The calculations have been carried out on a single processor INTEL 2.6 GHz processor. Computational time for one

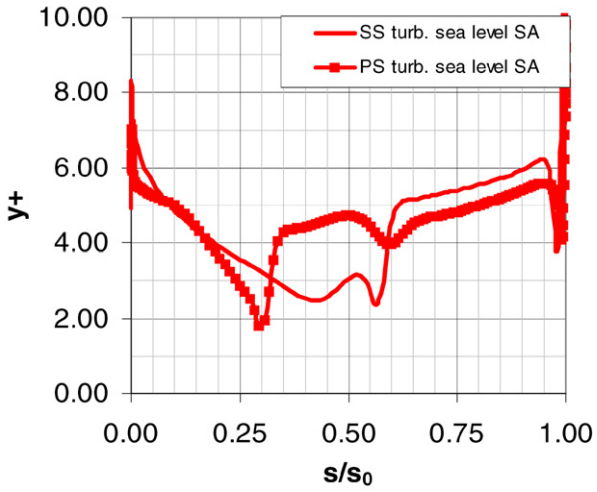

Fig. 4. y^+ values in the first cell above the blade surface on the suction side and pressure side.

Table 1
Boundary conditions

		Sea level	Altitude 51 kft
Inlet	p_{t1}	101 350 Pa	20208 Pa
	T_{t1}	288 K	227 K
	ν_{t1}	10e–4 m^2/s	10e–4 m^2/s
Outlet	p_2	86000	17150
		...	...
		108000 Pa	23000 Pa

operation point was in the order of 6 h, typically leading to a reduction in residual of 4 orders of magnitude.

7. Boundary conditions

In Table 1 the boundary conditions for both calculations are listed. Total pressure, total temperature, flow angle and turbulent intensity are prescribed at the inlet. The flow enters the calculation domain in axial direction. For the calculation of the characteristics (pressure ratio and efficiency versus mass flow) the exit pressure was varied. For that reason a simple radial equilibrium was applied for each of the applied pressures at the exit.

8. Results and comparison

Steady calculations with a fully turbulent and a transitional treatment of the boundary layer for two different operating altitudes are compared in the first subsection. An unsteady calculation with the transition model for the altitude case was added because of a significant change in the characteristic of the fan was found in the steady calculations. The results of the unsteady part of the investigations are discussed in the second subsection.

8.1. Steady investigation

Four compressor characteristics were calculated by increasing the backpressure step by step at the outlet of the computational domain. In the following diagrams the results for the

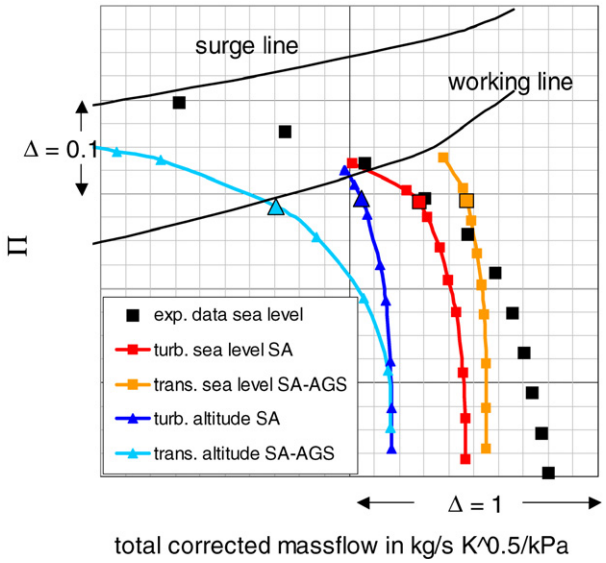

Fig. 5. Fan characteristic pressure ratio over reduced mass flow.

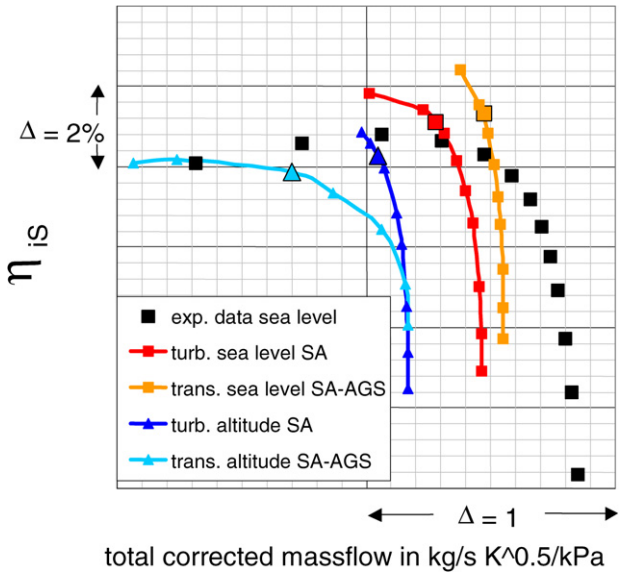

Fig. 6. Fan characteristic adiabatic efficiency.

sea level conditions and thus high Reynolds numbers are represented by red colour for the turbulent treatment of the boundary layer and by orange colour for the calculations with the Abu–Ghanam–Shaw transition model extension. The calculations under altitude conditions, which correspond to the low Reynolds number, are plotted in blue colour for the fully turbulent boundary layer calculations and in light blue for the transition model results.[1] Depending on the usage of the transition model and the operating conditions at sea level and altitude the characteristic of the fan changes (see Figs. 5 and 6).

Both the pressure ratio and the efficiency is increased by switching from the turbulent boundary layer calculation (red line) to the transition model (orange) at sea level conditions whilst the behaviour is vice versa for the altitude operating conditions (blue and light blue). The transition model (light blue) calculates smaller pressure ratios and poorer efficiencies near the working line at high altitudes and low Reynolds numbers respectively. It should be mentioned that the calculation of the flight case in high altitudes matches the behaviour of the scaled test rig experimental results (in house) best even though the mass flow is under predicted.

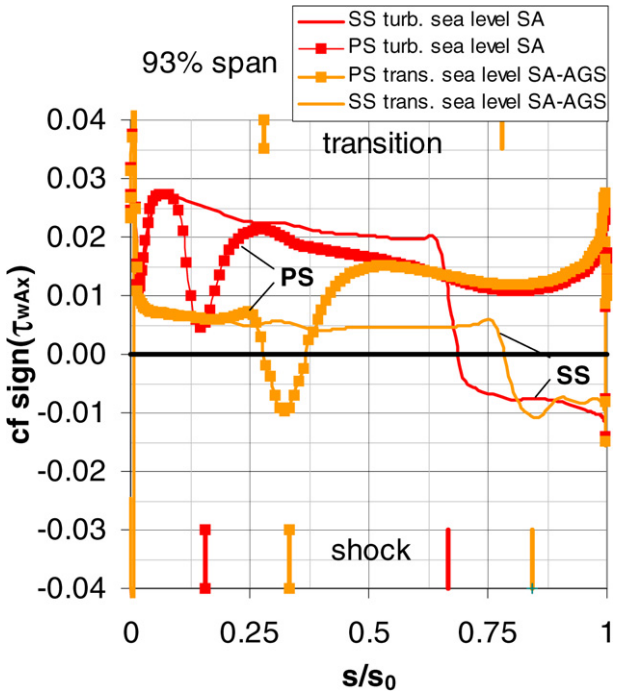

Fig. 7. Skin friction coefficient at fan blade surface at 93% span for sea level conditions ($Re = 2.3 \times 10^6$).

The total corrected mass flow is increased for the high Reynolds numbers cases and especially for the used transition model (orange line). It is known that high Reynolds numbers lead to thinner boundary layers and thus to a smaller blockage (see Wassel [12]). If the boundary layer is allowed to stay laminar as it is the case for the calculations with transition model (orange) the boundary layers can be even thinner (compared to the turbulent calculation) close to the leading edge and as a result of the reduced blockage the mass flow is increased.

To investigate the effect of the transition on the fan characteristic near the working line, the skin friction coefficients along the blade surface at 93% span are compared to each other in Fig. 7 for sea level conditions and in Fig. 8 for altitude conditions on the suction side (SS) and pressure side (PS) of the fan. The enlarged makers in the fan characteristic plots indicate the selected points for the comparison (see Figs. 5 and 6).

It is obvious that the choice of the transition model leads to a significant change in the wall stress distribution for both operating altitudes. The reduced shear stress at the first section of the blade especially for the sea level case (Fig. 7) is due to the laminar behaviour of the boundary layer. The skin friction coefficient values of the calculations with the transition model approximate to the turbulent solutions after the shock wakes impinge at the positions $s/s_0 = 0.4$ at the pressure side and $s/s_0 = 0.8$ at the suction side.

[1] For colours see the web version of this article.

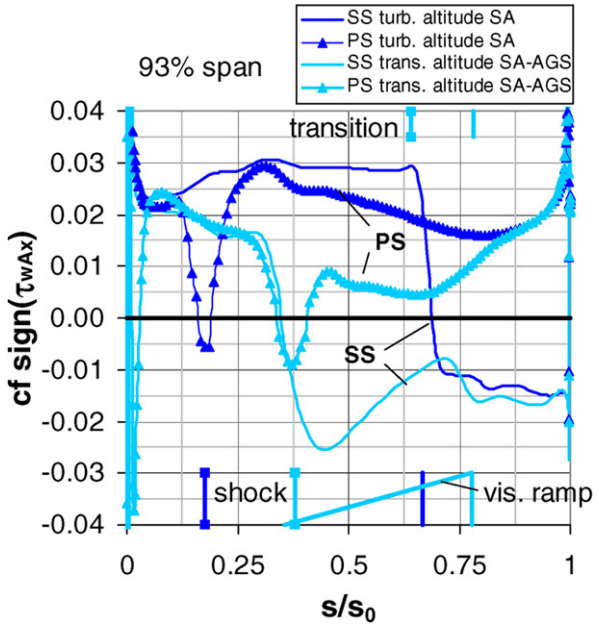

Fig. 8. Skin friction coefficient at fan blade surface at 93% span for altitude conditions ($Re = 5.05 \times 10^5$).

Further downstream where the boundary layer is turbulent in both calculations with the turbulence model and the transition model the skin friction coefficient values are in good agreement for sea level conditions. The kinks on the pressure side correspond to the indicated shock locations, which represent the relative Mach number lines of 1 close to the boundary layer. In the transition sea level case (orange) the skin friction coefficient falls underneath zero at $s/s_0 = 0.33$, which means that a small separation bubble is located under the shock. Because of the curvature of the blade at the pressure side the flow reattaches further downstream. On the suction side of the blade the flow separates after the shock impingement (fully turbulent $s/s_0 = 0.64$ and with transition model $s/s_0 = 0.84$). For the transition sea level calculation this occurs later and therefore the separation region is smaller (see Figs. 7 and 13). Due to the thinner boundary layer the shock moves further downstream in the passage (orange line).

This is not the case for the operating altitude of 51 kft (SS trans. altitude SA-AGS, light blue) where the skin friction coefficient falls below zero after an oblique shock attaches the suction side of the blade at $s/s_0 = 0.375$ (Fig. 8). The oblique shock is visible as the yellow region ahead of the shock in the relative Mach number plot in Fig. 10 ($Re = 5.06 \times 10^5$, trans. altitude). In Fig. 8 this region was named viscous ramp and is indicated by the light blue line in the bottom part of Fig. 8. It ends with the shock at $s/s_0 = 0.84$ where the transition takes place. Therefore the oblique shock starts at the location where the boundary layer is still laminar. In this region the laminar boundary layer separates from the suction side of the fan blade. The separation bubble is significantly increased compared to the calculation with fully turbulent boundary layer (see Figs. 8 and 13), which explains the higher blockage and thus the mass flow defect in the fan characteristic in Fig. 5.

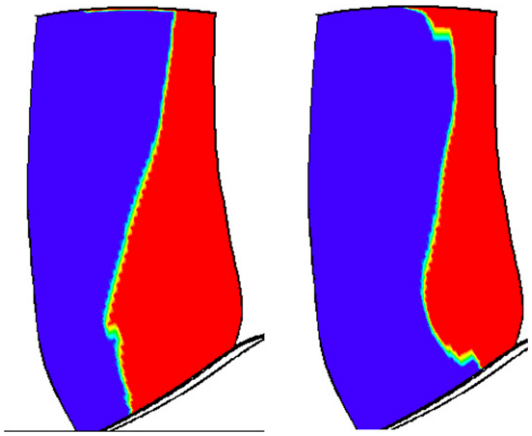

Fig. 9. Intermittency at suction side for sea level (left) and altitude (right), blue laminar, red turbulent boundary layer treatment. (For interpretation of the references to colour, the reader is referred to the web version of this article.)

Table 2
Location of transition

	Suction side (s/s_0)	pressure side (s/s_0)
Sea level	0.78	0.28
Altitude	0.78	0.64

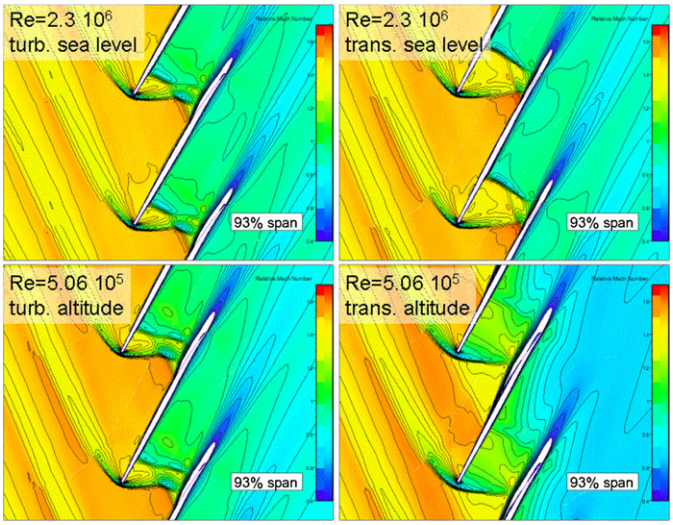

Fig. 10. Relative Mach number at 93% span.

Close to the shock position the transition from laminar to turbulent boundary layer occurs. It is assumed that the boundary layer transition is triggered by the shock. The existence of the laminar flow, represented by the blue colour, at the inlet of the blade is shown in Fig. 9 for the sea level and the altitude case. The locations of the transition is provided in Table 2.

Even for the high Reynolds number in the sea level case the boundary layer keeps laminar in the first part of the blade. The transition line moves downstream for the altitude conditions, as can be seen in the right contour plot in Fig. 9. Due to the lower Reynolds number the laminar boundary layer is extended further towards the trailing edge.

The shock position is shown in the plot of the relative Mach number in the blade to blade section at 93% span in Fig. 10.

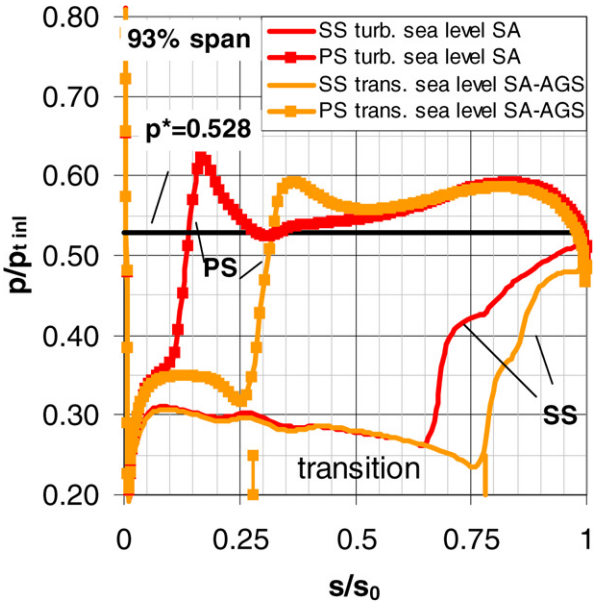

Fig. 11. Static pressure distribution on the fan blade surface at 93% span for sea level conditions.

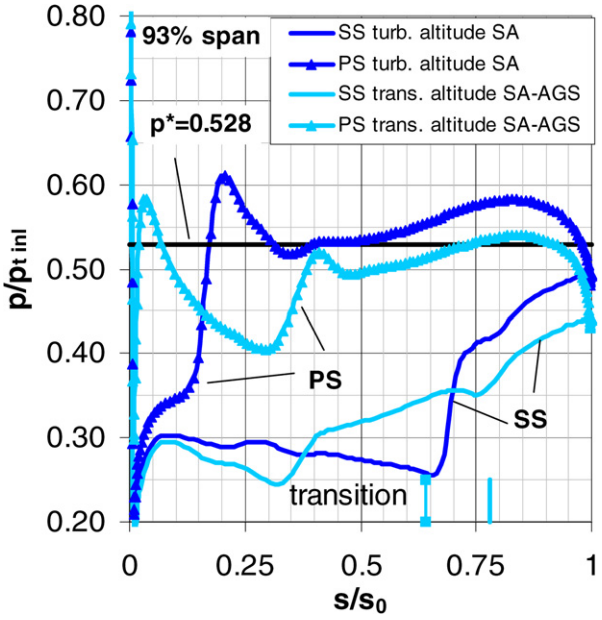

Fig. 12. Static pressure distribution on the fan blade surface at 93% for altitude conditions.

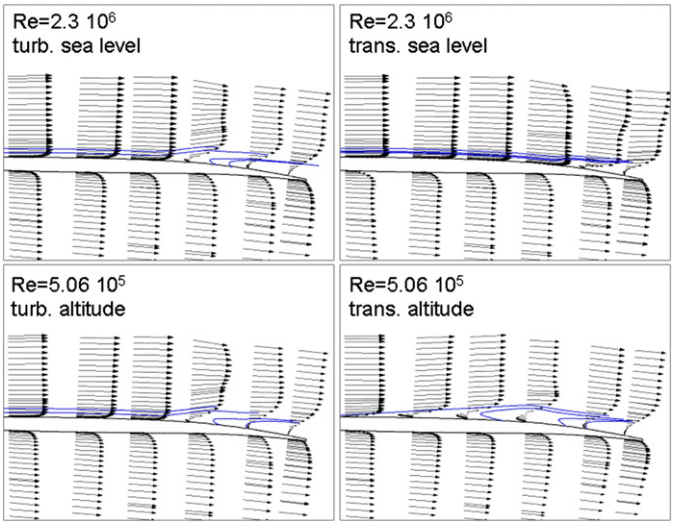

Fig. 13. Vector plots and iso lines at the trailing edge of the fan blade.

The location of the shock is changed significantly when the transition model is used. Further more the passage blocking moves downstream and increases the regions where boundary layer shock interactions take place. As mentioned before the laminar boundary layer interacts more sensitive with the shock than the turbulent boundary layer. Therefore the interaction region becomes bigger in the calculation with the transition model and the passage blocking moves further downstream. Further more the boundary layer thickness develops slower in the transition model calculations due to the consideration of the laminar boundary layer. Because of the thinner boundary layer at the passage inlet the minimum channel height is reached later than in the fully turbulent calculation. Especially in the altitude case with low Reynolds number the passage shock is changed close to the suction side. As also indicated by the plot of the skin friction a large separation bubble extends underneath the shock wave towards the leading edge. At the beginning of this separation an oblique shock takes place, which can be identified by the viscous ramp (yellow triangle) ahead of the main shock wave.

The static pressure was related to the total pressure at the stagnation point of the fan blade and was plotted for all investigated parameters to ascertain the differences in the characteristic of the fan stage (see Figs. 11 and 12). The additional black lines in the plots represent the pressure p^* where speed of sound is reached.

The shock is located at the intersection points of the pressure lines with the constant $p^* = 0.528$ line. The shock attaches the blade surfaces later when the transition model is used. This corresponds to the contour plots of the relative Mach number wherein the passage shock is located further downstream.

The flow especially in the tip region of the blade is more sensitive at low Reynolds numbers in the transitional simulation. This was also observed from Kügeler et al. [7] where a separation bubble and a lambda-type shock on the suction side of the DLR-TSG-97-cascade transonic profile was more pronounced in the computation with the transition model.

The separation bubbles are identified by the iso lines in the vector plot of the tangential component of the velocity in Fig. 13. Whilst the separation starts for the turbulent calculations more or less at the same point at 93% span, the behaviour in the transitional computation is completely different. In the sea level case the separation moves further downstream compared to the turbulent calculation. Under the altitude conditions the separation occurs significantly earlier for the calculations with the transition model. The onset of the laminar separation corresponds to the first kink on the suction side in the static pressure distribution in Fig. 12. More than 60% of the cord length of the blade the flow is separated from the suction side surface (see also Fig. 12). Therefore the blade to blade passage

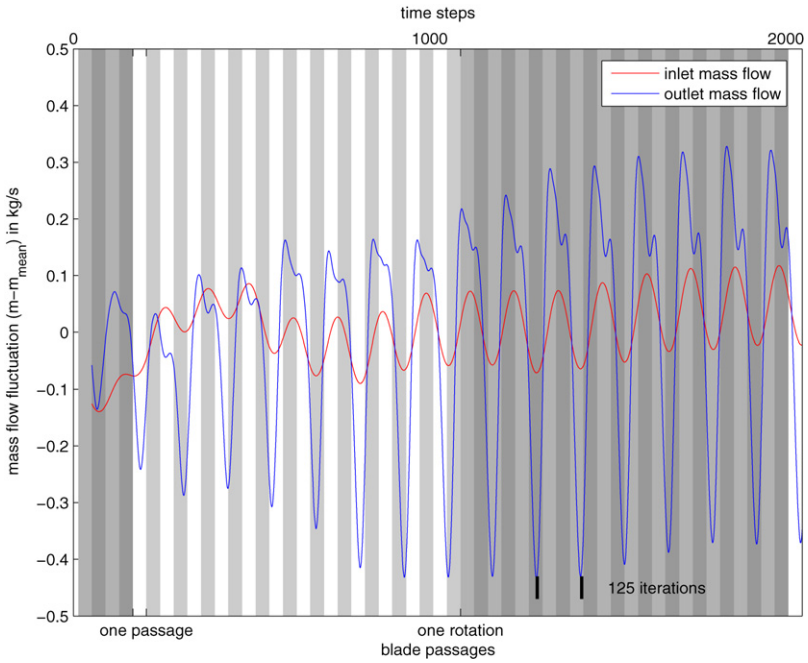

Fig. 14. Graphical representation of the mass flows at the inlet and outlet of the computational domain to characterise the time-dependent operating behaviour of the flow in the fan (high altitude transition model).

is blocked by the thickened boundary layer at the passage exit. This leads to the reduced mass flow in the fan characteristic at high altitude conditions and a penalty in the efficiency (see Fig. 5).

8.2. *Unsteady investigation*

Based on the results of the steady simulations, which demonstrate the time averaged impact of the Reynolds number on the fan characteristic, additional unsteady simulations of the altitude case with transition model were conducted to further investigate the dynamic behaviour. A detailed analysis of the unsteady results was performed to gain insights into the prevailing flow conditions, especially with regard to a further development of the fan to increase the efficiency and to guarantee a robust operating behaviour. The characteristic parameters describing the periodic, time-dependent operating behaviour of the BR710 fan are given by the rotation speed and the number of blades. For the simulated operating point this results in a Strouhal-number of $S_r = 0.109$ using the rotation speed and a Strouhal-number of $S_r = 2.609$ using the number of blades.

Fig. 14 displays the mass flow for two revolutions of the fan. Therein the blade passages (alternation of white and grey) and one revolution of the rotor (alternation of blue and transparent) are accentuated by different colours.

In contrast to the fluctuations in the mass flow at the inlet and outlet of the computational domain, which are also shown in Fig. 14, the frequencies of the time-dependent flow behaviour proved to be no multiple of the typical temporal parameters of the fan. From a Fourier-Analysis of these mass flow fluctuations, which are in-phase, a dominant Strouhal-number of $S_r = 0.8$ can be found. This corresponds to exactly 125 iterations of the time steps, which are used in the simulations. The cause of this very dynamic flow behaviour lies within the interaction of shock and boundary layer and is also influenced by the familiar phenomena occurring for the flow through the clearance at the top of the fan's blades.

For a better understanding of this behaviour, Fig. 15 displays the relative Mach number at 93% span for five characteristic times within the obtained dominant period. The selected time steps are representing the minimum and maximum values of the outlet mass flow and the efficiency. The evaluated time steps are indicated with numbers (1–5) in the first diagram, where the mass flow is plotted against the efficiency. The fluctuations in the tip region flow ends up in a variation of the overall efficiency of 1.5% and in a mass flow pulsation of 0.7 kg/s.

Starting with the highest mass flow and thus the lowest blockage in the passage at time step (1), the flow reaches the highest efficiency at point (2). The wake is the smallest in the evaluation plane at the rotor exit for this moment. At time step (3) the separated flow is weakened by the interaction of the shock with the tip vortex. The minimum mass flow and highest blockage of the flow represented by the strong wake can be obtained at time step (4). This strong wake is transported by the flow to the outlet of the computational domain and is responsible for the efficiency penalty at time step (5).

This dynamic behaviour is caused by the time dependent flow through the tip clearance, which in turn is decisively governed by the shock-boundary layer-configuration on the suction side of the blade.

The movement of the viscous ramp as a result of the shock-boundary layer interaction in combination with the tip vortex is provided by Fig. 16. The drop in the skin friction coefficient is an indicator for the beginning separation at the respective times (same numbers as in Fig. 15). At time step 3, when the tip vortex influences the separation most, the beginning of the

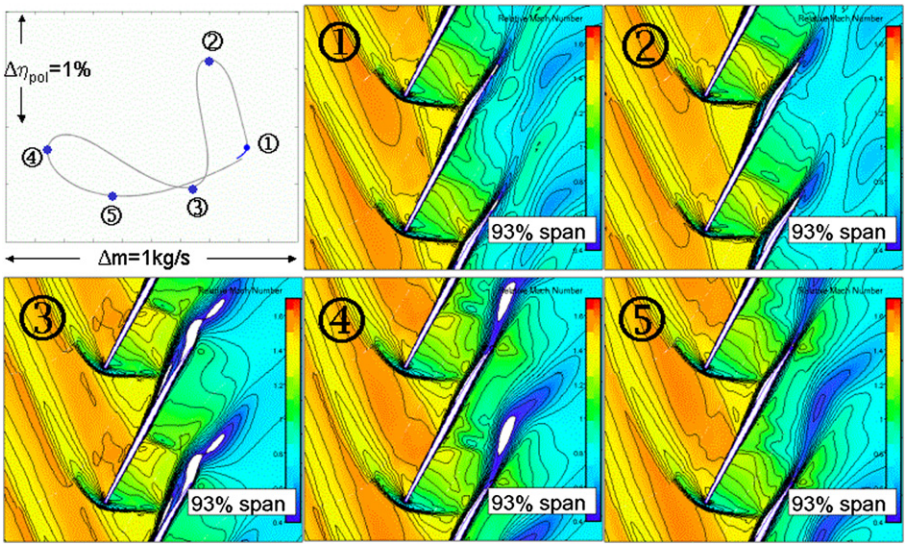

Fig. 15. Relative Mach number at 93% span for five selected time steps within one mass pulsation period (125 time steps) for the high altitude case with transition model ($Re = 5.06 \times 10^5$).

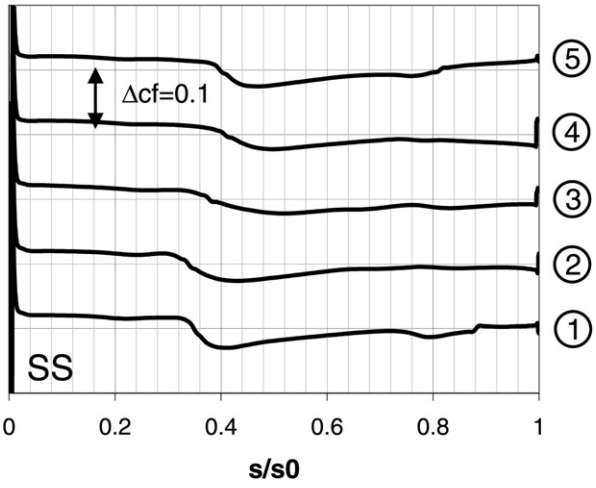

Fig. 16. Skin friction coefficient for the five time steps, which are displayed in Fig. 15.

viscous ramp is smoother and further downstream compared to earlier time steps. After the strong vortex in the rear part of the blade (see Fig. 15 time step 3) moves further downstream and away from the wall, the skin friction drop becomes stronger and the viscous ramp is moving back towards the leading edge.

These time-dependent fluctuations of the shock configuration trigger the periodic fluctuations in the mass flows at the inlet and even more at the outlet of the computational domain.

The strong fluctuations in the mass flows also entail load changes for the resulting forces, which in turn can cause flutter for critical operating points. By means of the results from these numerical simulations, preventive measures can be developed.

9. Summary and outlook

The present paper describes the complex impact of laminar-turbulent transition to shock boundary layer interactions. The physical effects in the interaction region are described in detail on the basis of surface pressure and laser measurements carried out on a transonic airfoil profile CAST 7. At the same free stream Mach number, the position of a shock on the airfoil is located further downstream in the case of free transition (i.e. laminar flow in front of the shock). Also, a laminar separation bubble develops far in front of the shock in the case of transitional shock boundary-layer interaction.

To assess these effects on a transonic fan blade a CFD package (NUMECA Int.) with a transition criterion was used. The transition model according to Abu-Ghanam and Show, which is described in detail, was implemented in the Spalart–Allmaras one-equation turbulence model. The BR710-fan was calculated in different operating conditions, i.e. at sea level altitude with high Reynolds number and in very high altitude, which represents the low level Reynolds number. For both cases fully turbulent and transitional computations were carried out for comparison reasons. Especially at low Reynolds number i.e. high altitude, the differences in the blade characteristics (pressure ratio and efficiency versus mass flow) are considerable. These are mainly caused by significantly different shock positions in both cases, which are caused by different throttling of the passage due to different boundary layer thickness. In the tip region of the blade the transition model implies a boundary layer separation, which is more pronounced than in the fully turbulent calculation. Therefore an unsteady investigation of the fan blade for the altitude operating conditions with transition model was performed.

It was found that the tip flow separates with a Strouhal-number of $S_r = 0.8$, which is not related to the blade passing frequency. The unsteady tip vortex interacts with the shock and thus with the transition location. As a result the periodic separating vortex decreases the efficiency and the mass flow through the machine.

Having these effects in mind it will be possible to design future fan blades which account for the real transitional shock boundary layer effects, especially at low Reynolds number operations.

References

[1] B. Abu-Ghanam, R. Shaw, Natural transition of boundary layers. The effects of turbulence, pressure gradient and flow history, J. Mech. Engrg. Sci. 22 (1980) 213–228.

[2] S. Dhawan, R. Narasimha, Some properties of boundary layer during the transition from laminar to turbulent flow motion, J. Fluid Mech. 3 (1958) 418–436.

[3] R.B. Ginder, W.J. Calvert, The design of an advanced civil fan rotor, ASME Trans. J. Turbomach. 109 (July 1987) 340–345.

[4] Th. Hildebrandt, M. Swoboda, E. Lorrain, Steady and unsteady transitional 3D Navier–Stokes calculation of a 1,5-stage axial low speed compressor, in: Proceedings of 17th International Symposium on Airbreathing Engines, 4–9 September 2005, Munich, Germany, 2005.

[5] A. Jameson, T.J. Baker, Multigrid solution of the Euler equations for aircraft configurations, AIAA Paper 84-00931984, 1984.

[6] E. Johann, M. Swoboda, T. Janetzke, W. Nitsche, Laminar to turbulent transitional behaviour of the boundary layer obtained from high speed rig test results and 3D Navier–Stokes calculation, to be presented on 18th International Symposium on Airbreathing Engines (ISABE), 2–7 September 2007, Beijing, China, 2007.

[7] E. Kügeler, A. Weber, S. Lisiewicz, Combination of a transition model with a two-equation turbulence model and comparison with experimental results, in: Proceedings 4th European Turbomachinery Conference, Florence, Italy, Paper No. ATI-CST-076/01, 2001.

[8] F.R. Menter, R.B. Langtry, S.R. Likki, Y.B. Suzen, P.G. Huang, S. Völker, A correlation-based transition model using local variables Part I and Part II, in: Proceedings of ASME Turbo Expo 2004, Power for Land, Sea and Air, Vienna, June 14–17, 2004.

[9] P.R. Spalart, S.R. Allmaras, A one-equation turbulence model for aerodynamic flows, AIAA-92-0439, 1992.

[10] M. Swoboda, W. Nitsche, Shock boundary-layer interaction on transonic airfoils for laminar and turbulent flow, J. Aircraft 33 (1) (January–February 1996).

[11] R.E. Walraevens, N.A. Cumpsty, Leading edge separation bubbles on turbomachinery blades, ASME Trans. J. Turbomach. 117 (1995) 115–125.

[12] A.B. Wassel, Reynolds number effects in axial compressors, J. Engrg. Power (April 1968) 149–156.